

# The long wavelength emission of interstellar PAHs: characterizing the spinning dust emission

Ysard N. and Verstraete L.

Institut d'Astrophysique Spatiale, UMR8617, Université Paris-Sud, F-91405, Orsay, France

Preprint online version: February 12, 2019

## ABSTRACT

**Context.** The emission of cold dust grains at long wavelengths will soon be observed by the Planck and Herschel satellites and will provide new constraints on the nature of interstellar dust. In particular the anomalous emission detected between 10 to 90 GHz, proposed to be due to small spinning grains (PAHs), should help to better define these species. Moreover, understanding quantitatively the fluctuations of the anomalous emission over the sky is crucial for CMB studies.

**Aims.** We focus on the long wavelength emission of interstellar PAHs in their rovibrational and rotational transitions. The PAH emission spectrum from the IR to the microwave range in standard interstellar phases is presented and compared to anomalous emission observations.

**Methods.** To model their long wavelength emission, we treat PAHs as isolated systems and follow consistently their IR (rovibrational) and rotational emissions. We consider several interstellar phases and discuss how the anomalous emission may constrain the PAH size distribution.

**Results.** Our model of PAH emission accounts for the mid-IR spectra of the diffuse interstellar medium and of the Orion Bar. We show that for  $\lambda \geq 3$  mm the PAH rovibrational emission does not scale any more with the radiation field intensity ( $G_0$ ) unlike the mid-IR part of the spectrum (which scales with  $G_0$ ). This emission represents less than 10% of the total dust emission at 100 GHz. Similarly, we find the broadband emissivity of spinning PAHs per carbon atom to be rather constant as long as  $G_0 \leq 100$  and for proton densities  $n_H < 100 \text{ cm}^{-3}$ .

**Conclusions.** Observations of anomalous emission in the Perseus molecular cloud are well explained by our model of PAH rotational emission with a standard abundance, supporting PAHs as the origin of the anomalous emission. The behaviour of the spinning dust emissivity with  $G_0$  provides a clear test that can be tested against observations of anomalous and dust mid-IR emissions. Comparison of these emissions will provide constraints on the size and/or electric dipole moment of interstellar PAHs.

**Key words.** dust, extinction – ISM: general

## 1. Introduction

The mid-IR spectrum of the interstellar medium (ISM) shows prominent bands from 3 to 17  $\mu\text{m}$  which account for one third of the energy emitted by interstellar dust. Such bands are emitted by very small (subnanometric) dust particles during internal energy fluctuations triggered by the absorption of a stellar photon (Sellgren 1984). The positions of these bands suggest the presence of aromatic, hydrogenated cycles in these grains. Léger & Puget (1984) and Allamandola et al. (1985) proposed Polycyclic Aromatic Hydrocarbons (PAHs) as the carriers of these bands. Despite two decades of experimental and theoretical efforts, the match (band positions and intensities) between data only available on small species and observations still remains elusive as illustrated recently by the work of Peeters et al. (2002) and Kim & Saykally (2002). Given their important role in the ISM (e.g., gas heating, Habart et al. (2001), UV extinction, Joblin et al. (1992)), it is necessary to find other ways to constrain the nature and size distribution of interstellar PAHs.

The Planck and Herschel data will soon trace the emission of cold interstellar grains in the interstellar medium. Due to their small size, PAHs are heated sporadically (every few months) by absorption of stellar photons and have a high probability to be in low-energy states (Draine & Li 2001). Interstellar PAHs

may thus contribute significantly to the emission at long wavelengths ( $\lambda > 1$  mm). In this context, an unexpected emission excess called *anomalous emission*, correlated to dust emission has been discovered between 10 and 90 GHz (Leitch et al. 1997; de Oliveira-Costa et al. 2002). In this spectral range several galactic emission components (synchrotron, free-free and thermal dust) contribute with a comparable magnitude and it is only recently that the anomalous emission has been separated in WMAP data (Miville-Deschênes et al. 2008). Spinning, small dust grains were first proposed by Draine & Lazarian (1998) (hereafter DL98) as a possible origin to this anomalous component. Since then analysis of observations has suggested that the anomalous emission is correlated to small grains (Lagache 2003; Casassus et al. 2006).

In this paper, we study the emission of PAHs with particular emphasis on the long wavelength part of the spectrum. In this spectral range, the emission is dominated by species in low-energy states for which each photon exchange represents a large energy fluctuation. To derive the internal energy distribution of PAHs, we use here the exact statistical method described in Draine & Li (2001). We take into account rotational states and include low-frequency vibrational bands in our cross-section. We present in a consistent fashion the rovibrational and broadband rotational emission of PAHs in a variety of interstellar phases. We compare our results to observations of anomalous emission and show how

the distribution of sizes and of electric dipole moment of interstellar PAHs can be constrained.

The paper is organized as follows. The second section describes the properties of PAHs adopted in this work. The third section discusses the internal energy distribution of PAHs and associated rovibrational emission. Sections 4 and 5 discuss the rotational excitation and emission of PAHs. Finally, conclusions and observational perspectives are given in the last section.

## 2. The properties of interstellar PAHs

In the ISM the most stable PAHs are found to be compact species (Léger et al. 1989; Le Page et al. 2003). Small PAHs are planar but above some size threshold (40 to 70 C atoms), interstellar formation routes may favor bowl- or cage-shaped species containing pentagonal cycles (see Moutou et al. (2000) and references therein). This threshold is not known however and the presence of fullerenes in the ISM is still elusive (Moutou et al. 1999). We therefore assume interstellar PAHs to be planar with a hexagonal ( $D_{6h}$ ) symmetry. The PAH radius is thus  $a(\text{\AA}) = 0.9\sqrt{N_C}$  where  $N_C$  is the number of carbon atoms in the grain (Omont 1986). The formula for such molecules is  $C_{6p^2}H_{6p}$  and their hydrogen-to-carbon ratio is  $\frac{H}{C} = f_H \sqrt{\frac{6}{N_C}}$  where  $f_H$  is the hydrogenation fraction of PAHs. In this work, we assume that PAHs are fully hydrogenated ( $f_H = 1$ ).

### 2.1. Absorption cross-section

The excitation, cooling and emission of PAHs depends on their absorption cross-section (Sect. 3) which we describe now. We take the visible-UV cross-section from Verstraete & Léger (1992) and apply their size-dependent cut-off for electronic transitions in the visible-NIR range. The resulting cross-section compares well to the available data (Joblin et al. 1992). In Tab.A.1, we discuss the mid-IR bands considered in this work. We assume that each vibrational mode is harmonic and that the corresponding band profile has a Drude shape (Draine & Li 2001) where the width is taken from astronomical spectra and the peak value is chosen so that  $\sigma\Delta\nu$  is equal to the value measured in the laboratory. By adopting the observed bandwidth, we empirically account for the complex molecular relaxation and band broadening (Pech et al. 2002; Mulas et al. 2006) in interstellar PAHs. Note that different definitions of the PAH IR cross-sections have been proposed by Rapacioli et al. (2005); Flagey et al. (2006) and Draine & Li (2006) from a decomposition of IR emission maps. We adopt here the band strength given in Pech et al. (2002) which were derived from laboratory data. We use the database of Mallocci et al. (2007) to define an average broadband cross-section of the far-IR vibrations of PAHs. At frequencies below  $500\text{ cm}^{-1}$ , each species features many modes but for compact species, they are found to accumulate in 3 definite frequency ranges: modes with a frequency of less than  $100\text{ cm}^{-1}$ , modes between  $100$  and  $200\text{ cm}^{-1}$  and modes between  $200$  and  $500\text{ cm}^{-1}$ . We therefore model the far-IR cross-section of compact PAHs with 3 modes (Tab. 1). The frequency of each mode is the mean of all modes falling within the given energy range weighted by their corresponding integrated cross-sections. We find that the frequency of the lowest energy mode depends on the molecular size as  $N_C^{-1}$  (see Fig. 1). Conversely, for the other two modes the mean energy is rather independent on size. The integrated cross-section of these 3 modes was estimated as follows. From the Mallocci database, we first derive the fraction of  $\sigma\Delta\nu$  for each of the 3 modes. Then, we assume that the total

**Table 1.** Far-IR rovibrational bands adopted in this work with the percentage of the total oscillator strength in each band. The last column indicates the in-plane (ip) or out-of-plane (op) character of the band. Similar bands were obtained for PAH neutrals.

$\lambda_{\text{cations}}$ ( $\mu\text{m}$ )	$\nu_{\text{cations}}$ ( $\text{cm}^{-1}$ )	$\Delta\nu$ ( $\text{cm}^{-1}$ )	$\sigma_i/N_C$ ( $10^{-20}\text{cm}^2$ )	% (cations)	Type
30.2	331	300	$9.6 \times 10^{-3}$	69.5	2/3 ip 1/3 op
74.1	135	100	$9.9 \times 10^{-3}$	23.9	2/3 ip 1/3 op
$4.9 \times N_C$	$2040/N_C$	100	$2.7 \times 10^{-3}$	6.6	2/3 ip 1/3 op

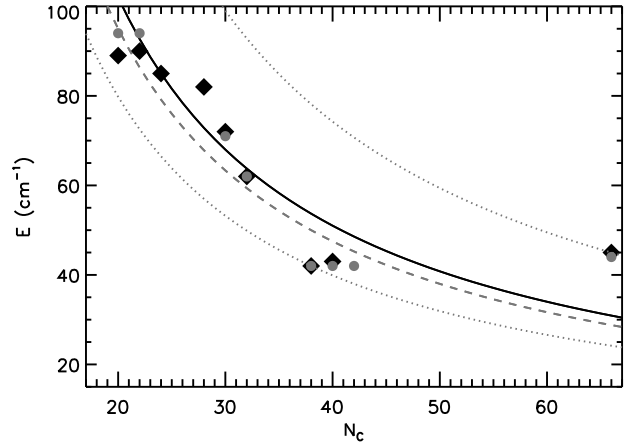


**Fig. 1.** Frequencies of the first (lowest energy) vibrational mode versus the number of carbon atoms  $N_C$  for PAH cations (black diamonds) and PAH neutrals (grey circles) from the Mallocci database (see text). The molecules considered are perylene ( $C_{20}H_{12}$ ), benzo[g,h,i]perylene ( $C_{22}H_{12}$ ), coronene ( $C_{24}H_{12}$ ), bisanthene ( $C_{28}H_{14}$ ), dibenzo[bc,ef] coronene ( $C_{30}H_{14}$ ), ovalene ( $C_{32}H_{14}$ ), circumbiphenyl ( $C_{38}H_{16}$ ), circumanthracene ( $C_{40}H_{16}$ ), cirumpylene ( $C_{42}H_{16}$ ) and circumovalene ( $C_{66}H_{20}$ ). The solid line is the relationship we adopt between the band position of cations and  $N_C$  and the dashed line shows the case of neutrals (see Tab. 1). The dotted lines show extreme cases for this relationship.

$\sigma\Delta\nu$  between 0 and  $500\text{ cm}^{-1}$  is given by the integral of the absorption cross-section  $\sigma_{\text{FIR}} = 4.3 \times 10^{-20} \lambda^{-1.24} \text{ cm}^2$  per C-atom (Schutte et al. 1993). The integrated cross-sections of each of the 3 modes is finally obtained by multiplying the former value by the  $\sigma\Delta\nu$  fractions from the database.

The far-IR bands adopted here are characterized in Tab. 1 and the full cross-section is displayed in Fig. 2. Finally, we note that the in-plane or out-of-plane character of each vibrational band is important because of their different weights in the rotational excitation (Sect.4.1). This character has been taken from Socrates (2001) and is indicated in Tabs. A.1 for the mid-IR bands. The character of the far-IR bands is less well known and we assume that one third and two thirds of the oscillator strength are from out-of-plane and in-plane transitions respectively (Tab. 1). We show in Sect. 3 that this set of IR bands provides a good match to observed interstellar spectra.

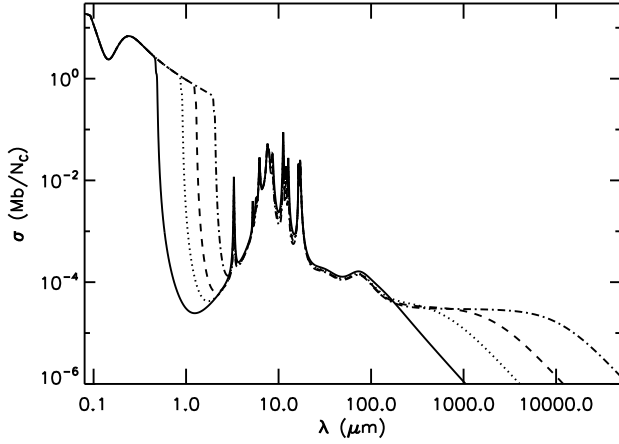


**Fig. 2.** The solid line is the absorption cross-section per carbon atom ( $1 \text{ Mb} = 10^{-18} \text{ cm}^2$ ) for cations with  $N_C = 24$ , the dotted line for  $N_C = 54$ , the dashed line for  $N_C = 96$  and the dot-dashed line for  $N_C = 216$ .

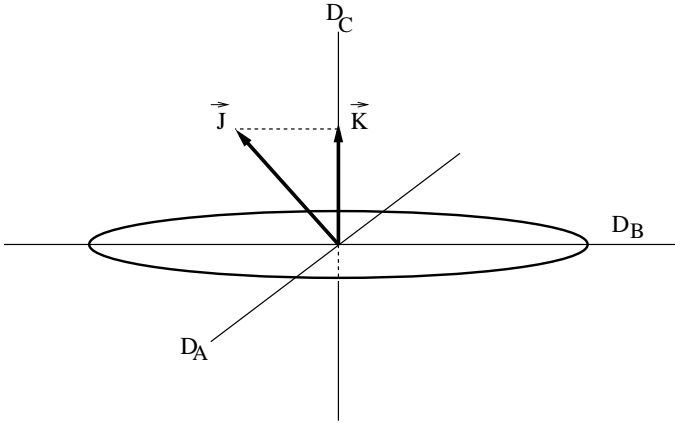


**Fig. 3.** Symmetric top molecule:  $D_A$ ,  $D_B$  and  $D_C$  are the principal axis of inertia and  $J$  is the total angular momentum of the molecule with  $K$  its projection along  $D_C$ .

## 2.2. The rigid rotor model

While describing the rotation of a molecule, the relevant operator is the total angular momentum  $\vec{J}$  which includes the electrons and nuclei contributions without the spin. We note  $D_A$ ,  $D_B$  and  $D_C$  the principal axis of inertia. We assume that PAHs are oblate symmetric top molecules with the axis  $D_C$  perpendicular to the plane of the molecule and parallel to  $Oz$ . We call  $I_C$  the inertia moment with respect to  $D_C$  and  $I_A$ ,  $I_B$  the inertia moments with respect to  $D_A$  and  $D_B$  which are taken to be parallel to  $Ox$  and  $Oy$ . The rotational hamiltonian is then:

$$H = \frac{J_x^2}{2I_A} + \frac{J_y^2}{2I_B} + \frac{J_z^2}{2I_C} \quad (1)$$

where  $J_x$ ,  $J_y$  and  $J_z$  are the projections of  $\vec{J}$  along the three inertia axis. Given the large number of carbon atoms in interstellar PAHs, we assume here that they are uniform disks with  $I_A = I_B = \frac{Ma^2}{4} = \frac{I_C}{2}$  (symmetric top) where  $M$  is the molecular mass. If we choose  $D_C \parallel Oz$ , we get:

$$H = \frac{J^2}{2I_B} + J_z^2 \left( \frac{1}{2I_C} - \frac{1}{2I_B} \right) \quad (2)$$

and the rotational energy is:

$$E_{rot} = BJ(J+1) + (C-B)K^2 \quad (3)$$

where  $B/hc = \frac{h}{4\pi c I_B} = 7 N_C^{-2} \text{ cm}^{-1}$  (neglecting the contributions of H to the molecular mass) and  $C = B/2$  are the rotational constants associated to  $D_B$  and  $D_C$ . The quantum number  $K$  is the absolute value of the  $J_z$ -eigenvalues. For a symmetric top molecule, the selection rules for rovibrational electric dipole transitions are:  $\Delta J = 0, \pm 1$  and  $\Delta K = 0, \pm 1$ . Writing the dipole moment as  $\vec{\mu} = \vec{\mu}_z + \vec{\mu}_B$  with  $\vec{\mu}_z$  along  $D_C$  and  $\vec{\mu}_B$  in the molecular plane along  $D_B$  (Townes & Schawlow 1975). Two kinds of transitions can be distinguished. First, the *parallel* transitions with  $\Delta K = 0$  and where the change of dipole moment in the transition is parallel to the top axis ( $D_C$ ) of the molecule. Second, the *perpendicular* transitions with  $\Delta K = \pm 1$  and where the change of dipole moment in the transition is perpendicular to  $D_C$ . Parallel transitions thus correspond to *out-of-plane* vibrations while perpendicular transitions correspond to *in-plane* vibrations.

Since the available microwave data are broadband observations ( $\lambda/\Delta\lambda$  of the order of a few), we make a number of simplifying assumptions in the description of the rotational motion of PAHs. We thus assume that the rotational constant  $B$  is the same in all vibrational levels and within the framework of a rigid rotor model we neglect the centrifugal distortion terms in the energy equation which are usually small for large molecules (Herzberg 1968ab; Lovas et al. 2005).

## 2.3. Electric dipole moment

The rotational emission of PAHs depends on their permanent electric dipole moment,  $\mu$ . Symmetric ( $D_{6h}$ ), neutral and fully hydrogenated PAHs have  $\mu \sim 0$ . Spectroscopic analysis of their IR emission bands suggests that interstellar PAH can be in cationic form, partially hydrogenated (Le Page et al. 2003) and maybe also substituted (Peeters et al. 2002, 2004a). For instance, a PAH having lost one H atom has  $\mu \sim 0.8$  to 1 D and a PAH cation where a C atom has been substituted by N would also have  $\mu \sim 0.1$  to 1.5 D depending on its size (T. Pino, private communication). Moreover, it has been proposed that non-planar PAHs containing pentagonal rings may exist in the ISM (see Moutou et al. (2000) and references therein): such species are known to have a large dipole moment as recently measured on coranulene,  $C_{20}H_{10}$ ,  $\mu = 2 \text{ D}$  (Lovas et al. 2005). In this work, we assume that interstellar PAHs electric dipole moment can be expressed as DL98:

$$\mu(N_C) = m \sqrt{N_{at}} + 4.3 \times 10^{-2} \sqrt{N_C} Z \sim m \sqrt{N_{at}} \quad (\text{Debye}) \quad (4)$$

where  $N_{at}$  is the total atoms number in the molecule,  $Z$  is its charge and  $m$  is a constant. Unless otherwise stated we will use  $m = 0.4 \text{ D}$ .

## 3. Internal energy distribution and rovibrational IR emission of isolated interstellar PAHs

After absorption of a visible-UV photon, each PAH cools off by emission of IR rovibrational photons. These photons reduce the angular momentum of the molecule and also, by recoil, may increase it. Previous studies mostly used a thermal description of molecular cooling. In fact since PAHs spend a large fraction of their time at low internal energies (see Fig. 4) their emission at long wavelength cannot be considered as a negligible

fluctuation. While estimating the emission of PAHs at low temperatures, the validity of a thermal approach is hence questionable. Because of the rapid energy redistribution after interactions (photon exchange or collisions with gas phase species), PAHs rapidly reach thermodynamical equilibrium while isolated (Léger et al. 1989). To describe this situation, we use here the exact statistical method of Draine & Li (2001) to derive the stationary internal energy distribution of PAHs,  $P(E)$ .<sup>1</sup>

The distribution  $P(E)$  depends on (a) the energy density of the exciting radiation field  $u_E = 4\pi\nu I_\nu$  (where  $I_\nu$  is the brightness), (b) the absorption cross-section  $\sigma$  of interstellar PAHs and (c) the rovibrational density of states  $\rho(E)$ . Unless otherwise stated, we use the local interstellar radiation field (Mathis et al. 1983) and scale it with a factor  $G_0$  equal to 1 in the case of the Mathis field<sup>1</sup>. In all cases we add the contribution of the CMB. The absorption cross-section used has been described previously. For simplicity, we did not include rotational bands. The density of states is obtained by first deriving the vibrational mode spectrum from a Debye model and then applying the Beyer & Swinehart (1973) algorithm for each molecular size (see Appendix B).

After each absorption of a stellar photon, we assume that the excitation energy of the PAH is rapidly redistributed among all the vibrational modes. This radiationless, isoenergetic process is called Internal Vibrational Redistribution<sup>2</sup> (IVR). The energy distribution is then computed according to the formalism (called exact statistical) described in Draine & Li (2001). The energy scale (referenced to the zero point energy) is divided into bins of energy  $E_i$  and width  $\Delta E_i$  with  $i = 0, 1, \dots, M$  ( $M = 500$ ) with  $0 \leq E_i \leq 2 \times 10^5 \text{ cm}^{-1}$ . When its energy is below that of the first excited vibrational state, the molecule is in a rotational state.  $P_i$  is the probability of having a grain in the bin  $i$  and the  $P_i$  are defined by :

$$\frac{dP_i}{dt} = \sum_{j \neq i} T_{j \rightarrow i} P_j - \sum_{i \neq j} T_{i \rightarrow j} P_i \quad (5)$$

where  $T_{j \rightarrow i}$  is the transition rate from the state  $j$  to the state  $i$  for a grain. We solve this equation in the stationary case. Further details can be found in Draine & Li (2001). Fig. 4 shows the energy distribution for three different radiation fields representative of molecular clouds, the diffuse interstellar medium (DIM) and the Orion Bar. We see that the most probable energy increases when the radiation field intensity  $G_0$  increases, as expected for PAHs whose cooling by IR emission is interrupted more frequently by absorption events. The sharp cut-off at  $\sim 1.1 \times 10^5 \text{ cm}^{-1}$  is due to the Lyman limit of photon energies in neutral regions. We also observe a tail at higher energies which is due to multiphoton events, i.e., absorption of a second photon while the PAH has not completely cooled off. This tail becomes more important as absorption events are more frequent, i.e., for large PAHs or intense radiation fields. Conversely we show in Fig. 4b that the radiation field hardness has little influence on  $P(E)$ . To estimate the effect of the rotational absorption we neglected, we included a rotational band centered at  $1 \text{ cm}^{-1}$  of width  $1 \text{ cm}^{-1}$  and corresponding to  $J = 150$  ( $\sigma/N_C \sim 9 \times 10^{-22} \text{ cm}^2/\text{C}$ ): we found  $P(E)$  to be affected between 1 and  $10 \text{ cm}^{-1}$  by less than a factor 2 and unchanged otherwise. This may change emission around  $1 \text{ cm}$  and at very low flux level. Conversely, the rotational excitation rates (section 4.1) which depends on the populations of excited vibrational levels are unaffected by this hypothesis.

<sup>1</sup>  $G_0$  scales the radiation field intensity integrated between 5 and 13.6 eV. The Mathis radiation field corresponds to an intensity of  $9.5 \times 10^{-5} \text{ erg/s/cm}^2/\text{sr}$ .

<sup>2</sup> The influence of this assumption is discussed in Appendix 3.1.

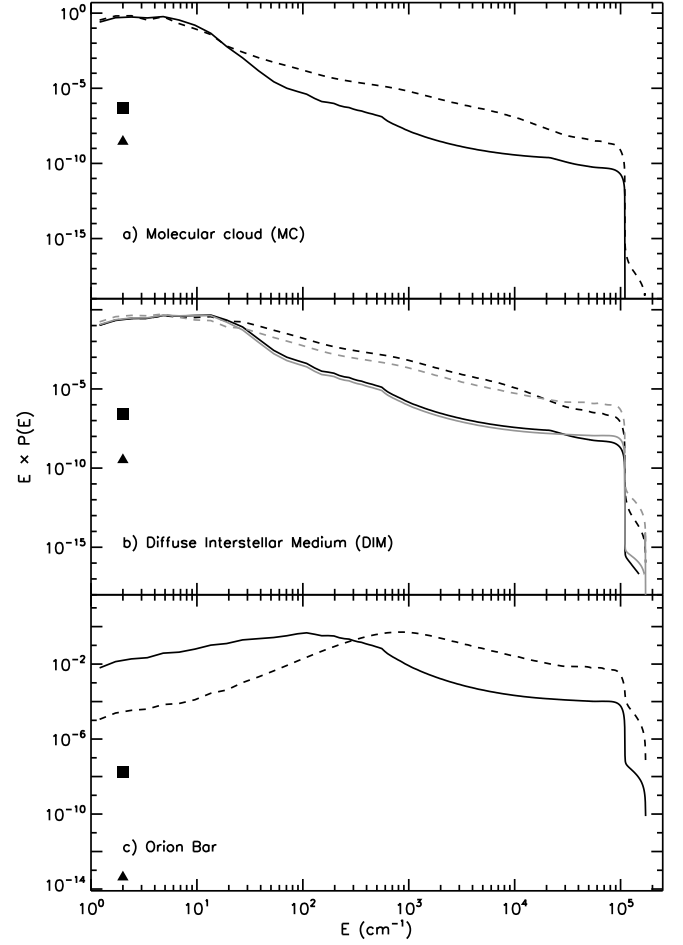


**Fig. 4.** Internal energy distribution  $P(E)$  of interstellar PAHs with  $N_C = 24$  (solid line and box for  $P(0)$ ) and  $N_C = 216$  (dashed line and triangle for  $P(0)$ ) in the case of *a*) molecular clouds or MC ( $G_0 = 10^{-2}$ ), *b*) the diffuse ISM or DIM ( $G_0 = 1$ ) and *c*) the Orion Bar where the radiation field is the sum of the CMB, the ISRF and a blackbody at 37 000 K corresponding to  $G_0 = 14,000$ . To illustrate the effect of the radiation field hardness, we show in *b*) the case of an Orion Bar type stellar radiation field scaled down to  $G_0 = 1$  (grey lines).

Knowing the internal energy distribution of PAHs, we can deduce the IR emission from upper state  $u$  by summing the contributions of all lower vibrational modes  $l$  (Draine & Li 2001):

$$\nu F_\nu = \frac{2h\nu^4}{c^2} \sigma(\nu) P(h\nu) \left( 1 + \frac{u_E}{8\pi h^3 \nu^3} \right) \quad (6)$$

$$\text{where } P(h\nu) = \sum_l P_l \sum_{u=0}^{l-1} \frac{g_u}{g_l} \Delta E_u G_{ul}(h\nu) + \sum_l P_l \left( 1 - \frac{h\nu}{\Delta E_l} \right) \quad (7)$$

is the number of rovibrational photons emitted at a given energy. The  $G_{ul}$  functions are defined in Draine & Li (2001). The degeneracies  $g_u$  and  $g_l$  are the numbers of energy states in bins  $u$  and  $l$  respectively (see Appendix B). Fig. 5 shows a comparison between observations and the PAH IR emission estimated

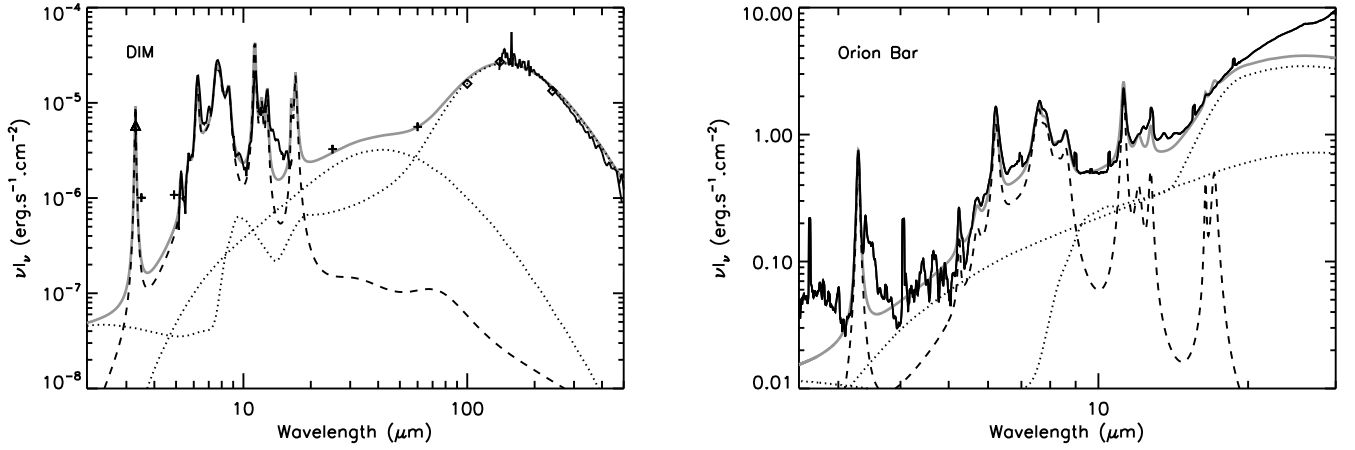


**Fig. 5.** *Left:* Dust Infrared emission of the DIM (solid thin lines and symbols) with a column density  $N_H \sim 10^{20} \text{ cm}^{-2}$  (Boulanger 2000). The total model dust emission is overlaid in bold grey. MRN type size distributions have been used for all dust populations. The PAH vibrational contribution (dashed line) is from the present model with  $N_C = [18, 96]$  with a 1:3 mixture of neutrals and cations, full hydrogen coverage and requires 43 ppm of carbon. In the cm-range, this emission is a 1000 times below the level of anomalous component (see Fig. 10). The contributions of larger grains are from an updated version of the Désert et al. model (Compiègne et al. 2008). The dotted line shows the contribution of graphitic Very Small Grains (VSGs) of radii  $a = 0.9$  to 4 nm containing 39 ppm of C. The dot-dashed line shows the contribution of silicate Big Grains (BGs) with  $a = 0.4$  to 250 nm using 37 ppm of Si. *Right:* Dust emission from the Orion Bar (the noisy dotted line is the ISO-SWS spectrum) with  $N_H \sim 1.8 \times 10^{21} \text{ cm}^{-2}$ . The model dust parameters are as above but for PAHs which are less abundant (18 ppm of C) and more ionized (82% are cations). Note the  $\sim 10 \mu\text{m}$  emission of small silicate grains also revealed by ISOCAM observations (Cesarsky et al. 2000).

with the present model and a size distribution  $n(a) \sim a^{-3.5}$  from Mathis et al. (1977) (hereafter MRN) which still is a good paradigm (Kim et al. 1994). We see that the emission of the DIM is well explained with a standard abundance of carbon in PAHs and an important fraction of cations as in Flagey et al. (2006). A similar good match is obtained for the Orion Bar spectrum with an important PAH depletion probably reflecting an efficient photodestruction in this excited environment. Fig. 6a shows that the mid-IR emission of PAHs scales with  $G_0$  while for  $\lambda > 2 \text{ mm}$  it is insensitive to  $G_0$  changes. In fact, the emission in this spectral range is contributed mostly by PAHs in low-energy states for which the dominant heating source is absorption of CMB photons: this is why this part of the spectrum does not vary much with  $G_0$ . However, while our model shows the broadband behaviour of the PAH emission we emphasize that if a detailed cross-section per molecule is used, the PAH emission at  $\lambda > 20 \mu\text{m}$  is a superposition of numerous narrow bands that may be detectable with the HIFI instrument onboard Herschel (Mulas et al. 2006).

### 3.1. Decoupling of vibrational modes

Our derivation of  $P(E)$  assumes an efficient energy redistribution between vibrational modes (IVR) during the PAH relaxation. IVR thus involves a coupling between vibrational modes via intramolecular transitions. However, it is known that IVR is no more efficient when the excitation energy is below some threshold  $E_{dec}$  (Mulas et al. 2006). When  $E < E_{dec}$ , the excitation of vibrational modes energetically accessible is frozen according to microcanonical statistics at energy  $E_{dec}$ . The molecule then continues cooling via emission in active or non-active vibrational modes.

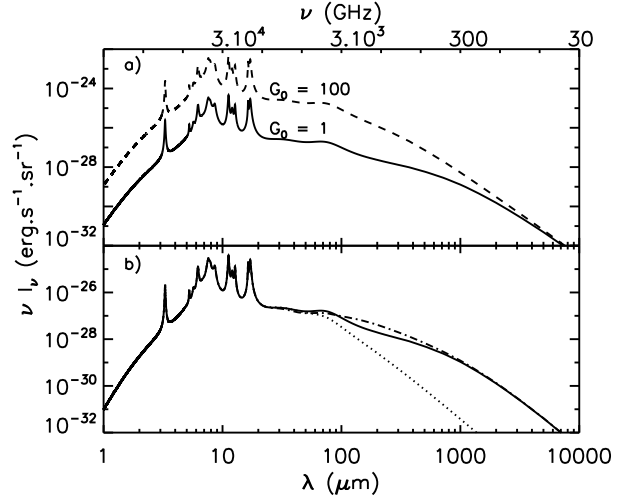


**Fig. 6.** PAH rovibrational emissivity for a MRN size distribution with  $N_C = 18 - 216$ . In a) we show the case of radiation field intensities corresponding to  $G_0 = 1$  and 100 and in b) we show illustrate the effect IVR breakdown, the dot line shows case 1 and the dot-dash line shows case 2 (see section 3.1).

To study here the influence of decoupling on the long wavelength emission we consider two extreme cases for the relaxation at  $E < E_{dec}$ :

- case 1: no IVR, cooling by IR forbidden modes. We assume these modes to be as of Tab. 1 but with an oscillator strength  $10^4$  lower
- case 2: no IVR, cooling only by the first vibrational mode at  $2040/N_C \text{ (cm}^{-1}\text{)}$  as defined in Tab. 1

and compare to our model with no decoupling (IVR always fulfilled). We take  $E_{dec}$  to be constant equal to  $500 \text{ cm}^{-1}$ , a

value representative for PAHs containing 20 to 30 carbon atoms (Joblin & Mulas 2008). In fact,  $E_{dec}$  is expected to decrease with molecular size because of the increasing density of states at a given energy (Mulas 1998): we therefore believe that the former cases provide an upper limit to the long wavelength emissivity of PAHs. Fig. 6b shows that as expected case 1 provides a lower limit to the long wavelength emission of PAHs while case 2 is an upper limit. Note that our IVR model is close to case 2. Moreover, in the case of the coronene cation ( $C_{24}H_{12}^+$ ), a comparison of our model (with IVR) band fluxes to the Monte-Carlo simulations of Joblin & Mulas (2008) shows a good general agreement, in particular for the low energy modes. At low spectral resolution, our far-IR to submm emission spectrum is also similar to that of Mulas et al. (2006). Our IVR model provides an upper limit to the broadband PAH rovibrational emission at  $\lambda > 3$  mm: the conclusions of the former section therefore hold even if the IVR hypothesis breaks down. We discuss in Appendix C the consequences of this hypothesis for the rotational excitation.

#### 4. Angular momentum distribution

The building of the angular momentum distribution of interstellar PAHs is driven by photon exchange and gas-grain interactions (DL98). In the DIM pervaded by the ISRF and for a PAH bearing 50 carbon atoms, the mean time between absorptions of visible-UV photons ( $\sim 0.2$  yr) is comparable to the mean time between emissions of rotational photons as well as to the mean time between PAH-hydrogen collisions (for a gas density  $100 \text{ cm}^{-3}$  and temperature  $100 \text{ K}$ ). Photons absorbed in the visible-UV make however a small contribution to the total angular momentum: indeed, given the fact that each photon carries a unit angular momentum, the numerous<sup>3</sup> IR photons emitted overwhelm the influence of the photon absorbed. To estimate the angular momentum distribution, we take the following processes into account:

- IR rovibrational photon emission
- purely rotational photon emission
- $H_2$  formation
- collisions with gas (neutral atoms and ions)
- plasma drag
- photoelectric effect

All these processes lead to a change of the angular momentum of the molecule and some of them excite the rotation and others damp it. As discussed by Rouan et al. (1997), the building of the angular momentum distribution  $n(J)$  can be considered as a stationary random walk in a potential well with a minimum for  $J = J_0$  where the rate of  $J$ -change is zero:

$$\left( \sum_i (\tau^{-1} \Delta J)_i \right)_{J_0} = 0 \quad (8)$$

with  $\Delta J$  the change of  $J$  produced by the event number  $i$  and  $\tau$  the mean time between two events  $i$ . As in Rouan et al. (1992), we assume an efficient Intramolecular Vibration to Rotation Energy Transfer (IVRET) and take  $n(J)$  to be the same for all vibrational levels equal to a Maxwell distribution  $n(J) = n_0 J^2 \exp(-J^2/J_0^2)$  where  $n_0$  is a normalization factor. Indeed, Mulas (1998) and Ali-Haïmoud et al. (2009) showed that this

form of  $n(J)$  was a good approximation. In the following, we establish the rate of  $J$ -change due to the rovibrational emission of isolated PAHs modelled in Sect. 3. We also present the rate of purely rotational photon emission while the contribution of the gas-grain interactions is described in Appendix E.

##### 4.1. Rovibrational transitions

The rovibrational IR emission can be as exciting as well as a damping process for the rotation of a PAH. Assuming that the interstellar PAHs are symmetric top molecules, the selection rules for the emission of one IR rovibrational photon are:  $\Delta J = 0, \pm 1$  and  $\Delta K = 0, \pm 1$ . We call  $W^+$ ,  $W^-$  and  $W^0$  the transition rates for the transitions  $\Delta J = +1$ ,  $\Delta J = -1$  and  $\Delta J = 0$  respectively. As seen in Sect. 2.2, two types of transitions are possible: parallel ones (out-of-plane vibrational motion) with  $\Delta K = 0$  and perpendicular ones (in-plane vibrational motion) with  $\Delta K = \pm 1$ . The type of each transition is given in Tab. A.1 and 1. For a rovibrational transition,  $(v, J, K) \rightarrow (v-1, J+\Delta J, K+\Delta K)$ , the rate is proportional to the spontaneous emission coefficient and to the probability for the grain to loose the corresponding transition energy. The spontaneous emission rate is proportional to  $A_{KJ}$  factors which represent the angular part of the transition probability. Formulae for these factors are given in Appendix D. Expressed in terms of cross-section, the transition rate is (with  $\nu_i$  and  $\Delta\nu_i$  in  $\text{cm}^{-1}$ ):

$$W_i^{\pm/0} = 8\pi c (\sigma_i \Delta\nu_i) \sum_{K=0}^J (\nu_i^{\pm/0})^2 A_{KJ}^{\pm/0} P(h\nu_i^{\pm/0}) \quad (9)$$

where the  $W_i^{\pm/0}$  give the transition rates for  $\Delta J = 0, \pm 1$  and for the transition  $i$  with a frequency  $\nu_i^{\pm/0}$  which depends on  $\nu_{i0}$  (the frequency of the vibrational band considered) and on  $J$  and  $K$  (see Appendix D). Since the  $J$ - and  $K$ -terms in  $\nu_i^{\pm/0}$  are always much smaller than  $\nu_{i0}$ , we will write  $P(h\nu_i^{\pm/0}) \simeq P(h\nu_{i0})$ . We note that in-plane transitions provide larger (by a factor  $\sim 2$ ) rates than the out-of-plane ones as a consequence of the  $A_{KJ}$  sum values. The total transition rates is obtained by summing over all bands:  $W^{\pm/0} = \sum_i W_i^{\pm/0}$ . Finally the rate of change of  $J$  due to rovibrational transitions is  $w = (\tau^{-1} \Delta J)_{IR} = W^+ - W^-$ . We find that rotational excitation dominates at low  $J$  whereas damping is the dominant process at high  $J$  values.

##### 4.2. Rotational emission

We consider here the spontaneous emission of purely rotational photons. The selection rules for such a transition are  $\Delta J = -1$  and  $\Delta K = 0$  (Townes & Schawlow 1975). No change of  $K$  occurs because for rotational transitions the dipole moment of a symmetric top molecule necessarily lies along its symmetry axis. The transition rate is then simply related to the spontaneous emission coefficient  $A_{J,J-1}$  and writes:

$$(\tau^{-1} \Delta J)_{rot} = -A_{J,J-1} \quad (10)$$

$$A_{J,J-1} = \frac{512\pi^4}{3h^4c^3} B^3 \mu^2 J^3 \frac{(2J+1)^2 - (J+2)}{3(2J+1)^2} \text{ s}^{-1} \quad (11)$$

where  $\mu$  is the dipole moment of the molecule and  $A_{KJ-}$  can be found in Appendix D<sup>4</sup>. Finally, the contribution of rotational

<sup>3</sup> Energy conservation thus imply that 40 IR photons are emitted after each absorption.

<sup>4</sup> In the high- $J$  limit,  $h\nu \times A_{J,J-1}$  tends to the classical expression of Larmor.

**Table 2.** Physical parameters for the typical interstellar phases considered in this work, namely the Cold and Warm Neutral Media (CNM and WNM) and the Warm Ionized Medium (WIM) which taken together make the Diffuse Interstellar Medium (DIM), Molecular Clouds (MC) and the Orion Bar as an archetypical photodissociation region. We note  $n_H$  the hydrogen density,  $T_{gas}$  the gas temperature,  $n_e$  the electrons density,  $n_{H^+}$  the proton density and  $n_{C^+}$  the density of atomic carbon ions.

	MC	CNM	WNM	WIM	Orion Bar
$G_0$	0.01	1	1	1	14 000
$n_H$ (cm <sup>-3</sup> )	300	30	0.4	0.1	10 <sup>4</sup>
$T_{gas}$ (K)	20	100	6000	8000	400
$n_e$ (cm <sup>-3</sup> )	0.03	0.045	0.04	0.1	3
$n_{H^+}/n_H$	0	$1.2 \times 10^{-3}$	0.1	0.1	$10^{-4}$
$n_{C^+}/n_H$	$10^{-4}$	$3 \times 10^{-4}$	$3 \times 10^{-4}$	$10^{-3}$	$2 \times 10^{-4}$

emission is<sup>5</sup>:

$$(\tau^{-1} \Delta J)_{rot} = -1.8 \times 10^{-14} \left( \frac{N_C}{50} \right)^{-6} \left( \frac{\mu}{1D} \right)^2 \times J^3 \frac{(2J+1)^2 - (J+2)}{(2J+1)^2} s^{-1} \quad (12)$$

#### 4.3. Equilibrium angular momentum $J_0$

We estimated damping and excitation rotational rates for the interstellar phases described in Tab. 2. Solving Eq. 8 we obtained the equilibrium angular momentum  $J_0$ . As in DL98, we find that, in all cases the damping is dominated by rotational and rovibrational emissions and that the excitation is provided by collisions with ions and neutrals and the photoelectric effect.

Fig. 7 shows that  $J_0$  increases with  $N_C$  for all the environments considered. Indeed the cross-section increases with size which means that the number of events in the random walk increases too. For the DIM, the cases of the CNM, the WNM and the WIM are similar. For a constant interstellar radiation field (ISRF here), a variation of the gas density and temperature has little influence on  $J_0$  ( $n_H = 0.1$  to  $30$  cm<sup>-3</sup> and  $T_{gas} = 100$  to  $8000$  K). In the case of the Orion Bar and molecular clouds,  $J_0$  is larger than in the DIM because the radiation field or the density is larger, again leading to a larger number of events in the random walk.

Observations of the mid-IR spectrum of PAHs in photodissociation regions and in the DIM indicate that a significant fraction of them is singly, positively charged (Verstraete et al. 2001; Flagey et al. 2006). Since the absorption cross-sections of PAH neutrals and cations are largely different, we examine here the influence of this quantity on  $J_0$ . We also consider variations of the frequency of the first vibrational mode. Fig. 7b shows that the  $J_0$ -values for PAH cations and neutrals are quite similar. In addition, changes of the relationship between the energy of the first vibrational mode and  $N_C$  are more noticeable in  $J_0$  for  $N_C > 100$  but stay below 10 %. From these results we conclude that the rotational excitation of PAHs is little sensitive to the shape adopted for the absorption cross-section.

The mid-IR rovibrational emission spectrum of PAHs is proportional to the incident radiation field intensity and also depends on its hardness (Verstraete et al. 2001): we therefore examine the influence of the exciting stellar radiation field on  $J_0$ . Using the  $G_0$  factor, we first scale the intensity of the radiation field

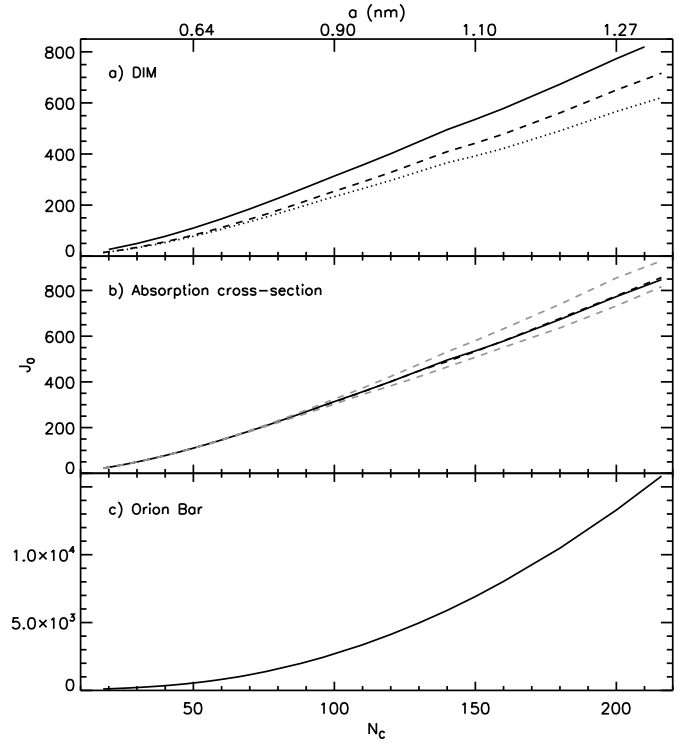


**Fig. 7.** Most probable angular quantum number  $J_0$  versus the PAH size. In a) we show the case of PAH cations in the DIM. Solid line shows the CNM, dashed line the WNM and dotted line the WIM. In b) we illustrate (CNM) the influence of the IR cross-section with the cases of PAH neutrals and cations (solid line for both) as well as that of extreme choices (see Fig. 1) for the relationship between the frequency of the first vibrational mode and  $N_C$  (gray dashed lines). In c), we present the case of the Orion Bar for cations.

taken to be a blackbody of effective temperature 22,000 K with  $10^{-2} \leq G_0 \leq 10^5$ . Fig. 8a displays the value of  $J_0$  versus  $G_0$  for  $n_H = 30$  cm<sup>-3</sup>. The gas state (temperature, electron, proton and C<sup>+</sup> abundances) has been determined with CLOUDY (<http://www.nublado.org>) at constant gas density<sup>6</sup>. There are two noticeable regimes in this plot. For  $G_0 \leq 10$  to 100 (depending on the size), the value of  $J_0$  is rather constant whereas for larger  $G_0$ , it increases. We also see that  $J_0$  increases faster for larger sizes. In fact when  $G_0$  or the size increases, the peak of  $P(E)$  moves towards the energy range of the first vibrational mode and the number of emitted vibrational photons increases leading to a larger  $J_0$  (there are more events in the random walk). For  $G_0 > 10$ , the mean time between absorptions of stellar photons<sup>7</sup> is shorter and the cooling of the molecule is interrupted. As a result, PAHs have a higher average internal energy (Fig. 4) and the probabilities for rovibrational transitions (Eq. 9) are enhanced as the peak of  $P(E)$  moves towards the energy range of the first vibrational mode. More rovibrational photons are then emitted and  $J_0$  rises (more steps in the random walk). We also observe in Fig. 8a that the  $G_0$ -threshold between the 2 regimes decreases with size: since the energy of the first vibrational mode

<sup>5</sup> In the limit  $J \gg 1$ , we estimated that the stimulated emission and absorption of CMB photons represent less than 20% of the spontaneous emission rate.

<sup>6</sup> The dust optical properties and abundances were defined as in Compiègne et al. (2008) and we used the following gas phase abundances [C] = 130, [N] = 75, [O] = 320, [S] = [Si] = 2 and [Fe] = 0.2 ppm.

<sup>7</sup> In the ISRF the mean time between absorbed photons is  $\tau_{abs} \sim 2.5 \cdot 10^8 (G_0 N_C)^{-1}$  seconds.

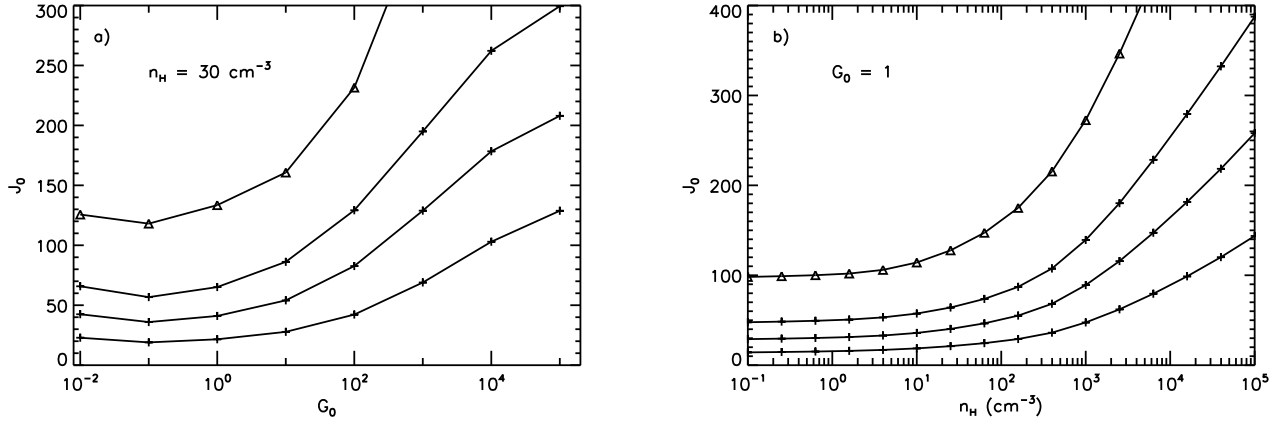


**Fig. 8.** *a)* Values of  $J_0$  for PAHs (cations) with  $N_C = 20, 30$  and  $40$  versus  $G_0$  (from bottom to top). The triangles show the  $J_0$ -values divided by 2 for  $N_C = 100$ . The gas density is  $30 \text{ cm}^{-3}$  and the other physical parameters for the gas are determined using CLOUDY (Ferland et al. 1998). *b)*  $J_0$  versus  $n_H$  for  $G_0 = 1$ . In both cases the radiation field is a blackbody with  $T_{eff} = 22\,000 \text{ K}$ .

of PAHs decreases with size, lower internal energy hence lower  $G_0$ -values are required to excite this mode. Finally, when the radiation field is harder (at given  $G_0$ ), the high-energy end of  $P(E)$  is enhanced (Fig. 4b) while still remaining low so that the  $J_0$ -value is little affected.

Fig. 8b shows the influence of gas density  $n_H$  on  $J_0$ -values. For  $n_H \lesssim 30 \text{ cm}^{-3}$ ,  $J_0$  is almost constant because the dominant processes (excitation by IR emission and rotational damping) do not depend on  $n_H$ . At larger  $n_H$ ,  $J_0$  increases because the rotational excitation is dominated by gas-grain interactions."

## 5. Spinning dust emission

The power emitted by a PAH containing  $N_C$  carbon atoms in a rotational transition from state  $J$  to  $J - 1$  is equal to:

$$P(J) = A_{J,J-1} \times 2BJ \quad (13)$$

taking the spontaneous emission rate  $A_{J,J-1}$  from Eq. 10 and with the transition energy  $h\nu = 2BJ$  ( $\Delta K = 0$  for rotational transitions). Since  $B \sim N_C^{-2}$ , we note that  $P(J) \sim N_C^{-8}$ . For a PAH size distribution  $n_{PAH}(N_C)$  (the number of PAHs per proton of radius between  $a$  and  $a + da$ ) and the angular momentum distribution  $n(N_C, J)$ , we get:

$$S_\nu = \frac{N_H}{4\pi} \int_{N_{min}}^{N_{max}} A_{J \rightarrow J-1} n(N_C, J) \frac{2BJ}{2Bc} n_{PAH}(N_C) dN_C \quad (14)$$

Since we are interested in a broadband spectrum we take the rotational bandwidth to be  $2Bc$ . As discussed before, we assume that  $n(N_C, J)$  is well described by a Maxwell distribution. In addition, given the relationship  $J_0(N_C)$  of Fig. 7, the size distribution and Eq. 14, the emission of spinning PAHs can be calculated. Fig. 9a & b show the case of an MRN type size distribution: the CNM, WNM and WIM have very similar emissivities. The rotational emission of PAHs depends on the abundance of small species ( $N_C \lesssim 70$ ) and on their permanent electric dipole moment,  $\mu$ . This latter is defined with  $m = 0.4 \text{ D}$  (see Eq. 4). We take the size distribution of PAHs to be a power law, i.e.,  $n_{PAH}(a) \sim a^{-\alpha}$  or  $n_{PAH}(N_C) \sim N_C^{-\beta}$  ( $\beta = (\alpha + 1)/2$ ) with the number of carbon atoms per molecule  $N_C$  taken to be between  $N_{min}$  and  $N_{max}$ . The fraction of small PAHs is thus determined by the choice of  $N_{max}$  or equivalently  $\alpha$ . As can be seen in Fig.

9a, the flux level of the rotational emission is sensitive to the small PAHs fraction in the size distribution. Cases with different fractions of small PAHs are shown in Fig. 9a where we vary  $\alpha$ . When  $\alpha$  increases the power emitted increases because the fraction of small PAHs ( $N_C \lesssim 70$ ) increases from 30% for  $\alpha = 0$  to 90% for  $\alpha = 6$  with  $N_{min} = 30$  and  $N_{max} = 216$ . In addition the emission spectrum is redshifted by 5 GHz and broadened by about the same amount when  $\alpha$  varies from 6 to 0. For a given size distribution, the flux level of the PAH rotational emission is proportional to:  $\int \mu^2 n_{PAH}(N_C) dN_C = m^2 \times S_{PAH}$  where  $S_{PAH}$  is the abundance per proton of PAHs. Detailed comparisons of model results to observations of anomalous and IR emission should therefore provide constraints on the abundance of PAHs and on the strength of their electric dipole moment.

## 6. The case of the molecular cloud G159.6-18.5

The anomalous emission that has been ascribed to spinning PAHs occurs in a spectral region (10-100 GHz) where several galactic emission components (synchrotron, free-free, thermal dust emission and CMB fluctuations) of comparable magnitudes are intermingled. Extracting the anomalous component on galactic scales involves the issue of component separation, the key step to obtain all-sky CMB fluctuations. Maximum entropy decompositions of the microwave sky performed by the WMAP team have shown that the synchrotron and anomalous components are difficult to separate and that low-frequency ( $\nu \leq 20 \text{ GHz}$ ) measurements provide important constraints in this respect (Finkbeiner et al. 2004; de Oliveira-Costa et al. 2004). Meanwhile, low-frequency observations towards selected targets where the synchrotron contribution is low have provided unambiguous detections of the anomalous component (Watson et al. 2005; Dickinson et al. 2006).

The COSMOSOMAS experiment has delivered maps of large sky fractions with an angular resolution of 1 degree in four frequency bands: 10.9, 12.7, 14.7 and 16.3 GHz. In this survey, Watson et al. (2005) studied the region G159.6-18.5 located in the Perseus molecular complex. Fig. 10 shows the spectrum of this region from 3 to 4000 GHz (COSMOSOMAS, WMAP and DIRBE data). From mid to far-IR, the Perseus molecular complex is dominated by a molecular ring (G159.6-18.5) surrounding an HII region. Unfortunately,

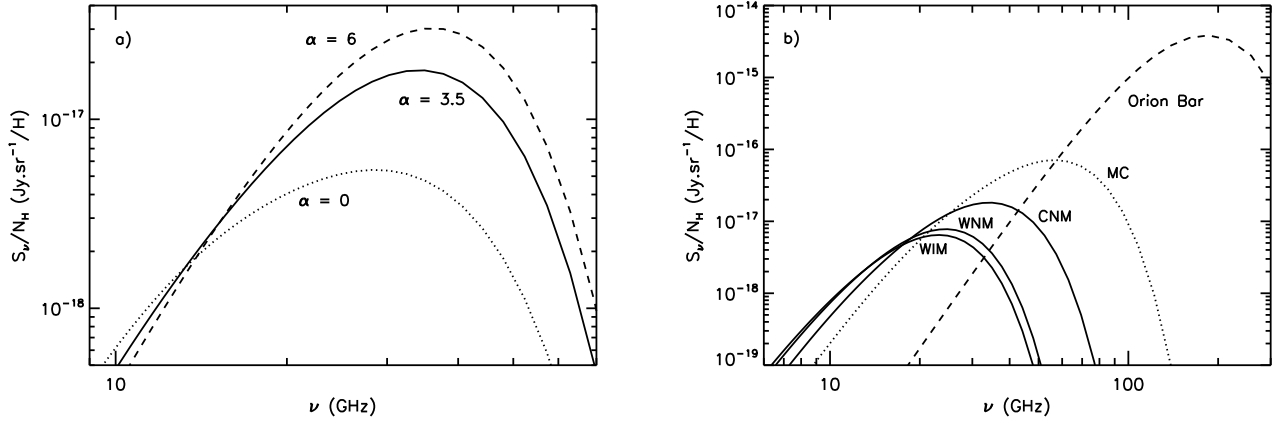


**Fig. 9.** Influence of the size distribution and of the interstellar environment on the rotational emissivity of PAH cations. We assume an electric dipole moment with  $m = 0.4$  Debye for all PAHs and a PAH abundance  $[C/H]_{PAH} = 4.3 \times 10^{-5}$ . *Panel a)* influence of the index  $\alpha$  of the power-law size distribution with  $N_C = [30, 216]$ . *Panel b)* rotational emission of a PAH size distribution with  $N_C = [30, 216]$  and  $n(a) \sim a^{-3.5}$ : solid lines represent the case of the DIM, dotted line that of MC and dashed line the Orion Bar.

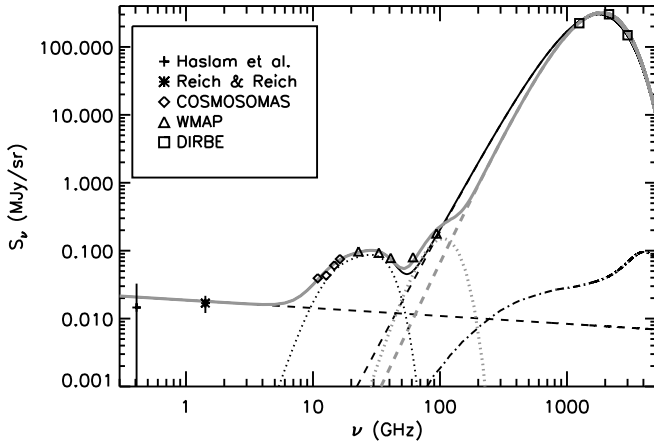


**Fig. 10.** Comparison to observations (symbols) of the Perseus molecular cloud G159.6-18.5 performed with COSMOSOMAS (Watson et al. 2005). The dashed lines show the free-free (low frequency) and big grains (high-frequency) emissions. The cloud total column density is taken to be  $N_H = 1.3 \times 10^{22} \text{ cm}^{-2}$  with a PAH abundance  $[C/H]_{PAH} = 2.4 \times 10^{-5}$  (see text). The PAH vibrational emission is represented by the triple dot-dashed line. The black model shows the fit when PAHs with  $N_C < 50$  are not present in the molecular ring (model 1) and the grey model presents the results when the smallest PAHs are included (model 2). See text for details.

the COSMOSOMAS resolution does not allow to separate these two phases. The molecular ring is centered on the star HD278942 (Andersson et al. 2000; Ridge et al. 2006). Its stellar wind is responsible for the HII region digged in the parent molecular cloud. To describe the emission G159-18.5, we assume it includes a MC component for the ring and a WIM component for the HII region.

We determine the physical parameters of both phases in the following way. According to Ridge et al. (2006), HD278942 is a B0 V star: the radiation field is modelled by the CMB and a blackbody with  $T_{eff} \sim 30\,000$  K, scaled to get  $G_0 \sim 1.6$  at the radius of the ring ( $G_0$  is determined with IRAS data). The radius

of the ring is approximately 2.75 pc (Andersson et al. 2000). For a B0 V star to dig an HII region of this size with its stellar wind, Ridge et al. (2006) estimated that  $n_H \sim 0.1 \text{ cm}^{-3}$ : we therefore adopt this density for the WIM. Andersson et al. (2000) have estimated the density and temperature of the gas in the molecular ring:  $n_H/G_0 \sim 350 \text{ cm}^{-3}$  or  $n_H \sim 560 \text{ cm}^{-3}$  and  $T_{gas} = (20 \pm 10)$  K. We determined the relevant gas phase abundances (for electrons, protons and  $C^+$ ) and the gas temperature ( $T_{gas} \sim 7\,500$  K) with CLOUDY. Watson et al. (2005) estimate the total column density (MC+WIM) to be  $N_H = 1.3 \times 10^{22} \text{ cm}^{-2}$ . From 12  $\mu\text{m}$  IRAS data and our PAH emission model, we estimate the total PAH abundance to be  $[C/H] = (2.4 \pm 0.4) \times 10^{-5}$ . If the thermal dust emission is represented as in Watson et al. (2005) by a grey body at 19 K with an emissivity index  $\beta = 1.55$ , our best fit parameters for the spinning PAH contribution, assuming a MRN type size distribution, are (model 1):  $N_C = 50 - 216$  and  $N_H = 4.6 \times 10^{21} \text{ cm}^{-2}$  for the MC,  $N_C = 24 - 216$  and  $N_H = 8.1 \times 10^{21} \text{ cm}^{-2}$  for the WIM. In both media we took  $m = 0.6$  D (Eq. 4). We note that PAHs are required to be larger in the MC, possibly as a consequence of grain-grain coagulation.

However, the results of Dupac et al. (2003) indicate that emission of dust around 20 K requires a higher emissivity index close to 2. In fact, adopting  $\beta = 2$  and a dust temperature of 18 K, we find an equally good fit of this region in the far-IR (Fig. 10, model 2). In this case the flux around 100 GHz is not explained. We speculate here that it may be due to an additional population of small PAHs in the MC component with:  $N_C = 24_{50}$ ,  $m = 0.1$  and  $N_H = 1.25 \times 10^{21} \text{ cm}^{-2}$  (for the larger PAHs in the MC phase,  $N_H = 4.25 \times 10^{21} \text{ cm}^{-2}$ ). The corresponding rotational emission is shown in Fig. 10 (model 2). The PAH size distribution would thus be bimodal, as already suggested by Le Page et al. (2003). As can be seen in Fig. 10, both models provide a good fit to the data. More clearcut tests of such scenarii will be soon possible with the Planck-Herschel data.

As can be seen on Fig. 10, both models provide a good fit to the data. Polarization data from Planck will help discriminate these scenarios: indeed, small grains or PAHs at the origin of the spinning emission are expected to be poorly aligned (Lazarian & Draine 2000a) whereas big grains are rather well aligned yielding a polarization fraction of 5 to 10%.

## 7. Summary

Due to their small size, interstellar PAHs spend most of their time at low internal energy and can spin at frequencies of 10 to 100 GHz. Recent observations have shown the existence of a 10-100 GHz emission component (the anomalous emission) related to the smallest grains of the interstellar dust population, the Polycyclic Aromatic Hydrocarbons or PAHs. As suggested by DL98, the anomalous emission may trace the emission of spinning PAHs.

In this paper, we discussed the long-wavelength (far-IR to centimetre range) emission of interstellar PAHs. To do so, we have treated PAHs as isolated systems and followed the internal energy distribution of PAHs down to very low energies ( $\sim 1$  wavenumber) because emission of GHz photons can then arise from fluctuations. In addition, we define the mid-IR vibrational bands as constrained from ISO and Spitzer data. To this band set, we have added low-frequency bands ( $\lambda > 20 \mu\text{m}$ ) through which PAHs cool at intermediate to low energies and which are important in describing their rotational emission.

We show that the rovibrational emission of PAHs above  $\sim 3$  mm is little sensitive to the intensity of the radiation field (represented here by  $G_0$ ) whereas the mid-IR part of the spectrum scales linearly with it. In the diffuse interstellar medium, PAHs may thus contribute up to 10% of the dust emission around 100 GHz. The rotational emission of PAHs is determined by the distribution  $n(J)$  of the angular momentum  $J$  of the molecule. As a function of molecular size, we find  $n(J)$  from a random walk formalism including all processes participating to rotational excitation and damping, namely, rovibrational and pure rotational emissions and gas-grain interactions. These processes depend on the local physical conditions (density and temperature of the gas, radiation field). We have therefore considered several interstellar environments. We derive the rotational emission of PAHs with a power-law size distribution of index  $\alpha$ . The emergent spectrum is dominated by the contribution of the smallest species and depends on the fraction of small PAHs (fixed by  $\alpha$ ) and how small they are, as set by the PAH minimal size  $N_{\min}$  (the number of carbon atoms in the smallest species). The emission of spinning PAHs also depends on their permanent electric dipole moment,  $\mu$ , a quantity difficult to infer from our present knowledge of interstellar PAHs. Comparing our model to observations of anomalous emission, we constrain  $N_{\min}$ ,  $\alpha$  and  $\mu$ . We also show that the rotational emissivity of PAHs is little sensitive to the intensity of the radiation field over the range  $G_0 = 0.1$  to 100.

These results open a number of perspectives. First, a systematic comparison between mid-IR and microwave data in selected, well-known targets will further test the origin of the anomalous emission. Such a project relies on a quantitative separation of microwave emission components that uses physical models for each of them. In this issue, as shown recently by Miville-Deschênes et al. (2008) (see also Battistelli et al. 2006), the polarisation of the microwave emission will provide important clues<sup>8</sup>. An observed correlation between the IR emission of PAHs and the anomalous emission compared to the present model predictions will provide an estimate of the PAH electric dipole moment  $\mu$  and of its variations with physical conditions. The abundance of PAHs required to explain the level of anomalous emission could then be derived and compared to that inferred from the IR emission. In addition, the spectral shape of the anomalous emission will constrain the PAH size range. The

anomalous emission may thus directly probe the properties of the interstellar PAHs which play an important role in the ISM but still resist quantitative characterization on the basis of IR spectra. We have started such a programme and present our results in a companion paper.

*Acknowledgements.* We gratefully acknowledge stimulating discussions with B. Draine, C. Joblin, E. Dartois, T. Pino and O. Pirali. We are grateful to M. Compiègne for his help in the dust SED modelling.

## References

- Ali-Haïmoud, Y., Hirata, C. M., & Dickinson, C. 2009, MNRAS, 405
- Allamandola, L. J., Tielens, A. G. G. M., & Barker, J. R. 1985, ApJ, 290, L25
- Andersson, B.-G., Wannier, P. G., Moriarty-Schieven, G. H., & Bakker, E. J. 2000, AJ, 119, 1325
- Baer, T. & Hase, W. 1996, Unimolecular reaction dynamics : theory and experiments (Oxford university press)
- Bakes, E. L. O. & Tielens, A. G. G. M. 1994, ApJ, 427, 822
- Beyer, T. & Swinehart, D. 1973, Comm. of the ACM, 16
- Boulanger, F. 2000, in ESA SP-455: ISO Beyond Point Sources: Studies of Extended Infrared Emission, ed. R. J. Laureijs, K. Leech, & M. F. Kessler, 3–4
- Casassus, S., Cabrera, G. F., Förster, F., et al. 2006, ApJ, 639, 951
- Cesarsky, D., Jones, A. P., Lequeux, J., & Verstraete, L. 2000, A&A, 358, 708
- Compiègne, M., Abergel, A., Verstraete, L., & Habart, E. 2008, A&A, 491, 797
- de Oliveira-Costa, A., Tegmark, M., Davies, R. D., et al. 2004, ApJ, 606, L89
- de Oliveira-Costa, A., Tegmark, M., Finkbeiner, D. P., et al. 2002, ApJ, 567, 363
- Dickinson, C., Casassus, S., Pineda, J. L., et al. 2006, ApJ, 643, L111
- Draine, B. T. & Lazarian, A. 1998, ApJ, 508, 157
- Draine, B. T. & Li, A. 2001, ApJ, 551, 807
- Draine, B. T. & Li, A. 2006, ArXiv Astrophysics e-prints
- Dupac, X., Bernard, J.-P., Boudet, N., et al. 2003, A&A, 404, L11
- Ferland, G. J., Korista, K. T., Verner, D. A., et al. 1998, PASP, 110, 761
- Finkbeiner, D. P., Langston, G. I., & Minter, A. H. 2004, ApJ, 617, 350
- Flagey, N., Boulanger, F., Verstraete, L., et al. 2006, A&A, 453, 969
- Habart, E., Verstraete, L., Boulanger, F., et al. 2001, A&A, 373, 702
- Herzberg, G. 1968ab, Diatomic Molecules (a), IR and Raman Spectra of Polyatomic Molecules (b) (Van Nostrand)
- Joblin, C., Boissel, P., Leger, A., D'Hendecourt, L., & Defourneau, D. 1995, A&A, 299, 835
- Joblin, C., Leger, A., & Martin, P. 1992, ApJ, 393, L79
- Joblin, C. & Mulas, G. 2008, in School on dust, Les Houches, ed. F. Boulanger, EAS Publication Series
- Jura, M. 1975, ApJ, 197, 575
- Kim, H.-S. & Saykally, R. J. 2002, ApJS, 143, 455
- Kim, S.-H., Martin, P. G., & Hendry, P. D. 1994, ApJ, 422, 164
- Lagache, G. 2003, A&A, 405, 813
- Lazarian, A. & Draine, B. T. 1999, ApJ, 516, L37
- Lazarian, A. & Draine, B. T. 2000a, ApJ, 536, L15
- Lazarian, A. & Draine, B. T. 2000b, ApJ, 536, L15
- Le Page, V., Snow, T. P., & Bierbaum, V. M. 2003, ApJ, 584, 316
- Léger, A., D'Hendecourt, L., & Defourneau, D. 1989, A&A, 216, 148
- Léger, A. & Puget, J. L. 1984, A&A, 137, L5
- Leitch, E. M., Readhead, A. C. S., Pearson, T. J., & Myers, S. T. 1997, ApJ, 486, L23+
- Lovas, F. J., McMahon, R. J., Grabow, J.-U., et al. 2005, J. Am. Chem. Soc., 127, 4345
- Mallocci, G., Joblin, C., & Mulas, G. 2007, Chemical Physics, 332, 353
- Martin, P. G. 2007, in EAS Publications Series, Vol. 23, EAS Publications Series, 165–188
- Mathis, J. S., Mezger, P. G., & Panagia, N. 1983, A&A, 128, 212
- Mathis, J. S., Rumpl, W., & Nordsieck, K. H. 1977, ApJ, 217, 425
- Miville-Deschênes, M.-A., Ysard, N., Lavabre, A., et al. 2008, A&A, 490, 1093
- Moutou, C., Sellgren, K., Verstraete, L., & Léger, A. 1999, A&A, 347, 949
- Moutou, C., Verstraete, L., Léger, A., Sellgren, K., & Schmidt, W. 2000, A&A, 354, L17
- Mulas, G. 1998, A&A, 338, 243
- Mulas, G., Mallocci, G., Joblin, C., & Toubanc, D. 2006, A&A, 460, 93
- Omont, A. 1986, A&A, 164, 159
- Pech, C., Joblin, C., & Boissel, P. 2002, A&A, 388, 639
- Peeters, E., Allamandola, L. J., Bauschlicher, Jr., C. W., et al. 2004a, ApJ, 604, 252
- Peeters, E., Hony, S., Van Kerckhoven, C., et al. 2002, A&A, 390, 1089
- Peeters, E., Mattioda, A. L., Hudgins, D. M., & Allamandola, L. J. 2004b, ApJ, 617, L65

<sup>8</sup> PAHs are expected to be poorly aligned in the ISM on observational (Martin 2007) and theoretical grounds (Rouan et al. 1992; Lazarian & Draine 2000b).

- Rapacioli, M., Joblin, C., & Boissel, P. 2005, A&A, 429, 193  
 Ridge, N. A., Schnee, S. L., Goodman, A. A., & Foster, J. B. 2006, ApJ, 643, 932  
 Roche, P. F., Lucas, P. W., & Geballe, T. R. 1996, MNRAS, 281, L25  
 Rouan, D., Leger, A., & Le Coupanec, P. 1997, A&A, 324, 661  
 Rouan, D., Leger, A., Omont, A., & Giard, M. 1992, A&A, 253, 498  
 Schutte, W. A., Tielens, A. G. G. M., & Allamandola, L. J. 1993, ApJ, 415, 397  
 Smith, J. D. T., Dale, D. A., Armus, L., et al. 2004, ApJS, 154, 199  
 Smith, J. D. T., Draine, B. T., Dale, D. A., et al. 2007, ApJ, 656, 770  
 Socrates, G. 2001, IR and Raman characteristic group frequencies : Tables and charts (John Wiley & Sons)  
 Townes, C. & Schawlow, A. 1975, Microwave Spectroscopy (Dover Publications)  
 Tripathi, A. K. and Sahasrabudhe, A., Mitra, R., Mukhopadhyay, R., Gupta, N., & Kartha, V. 2001, Phys. Chem. Chem. Phys., 3, 449  
 Verstraete, L. & Léger, A. 1992, A&A, 266, 513  
 Verstraete, L., Pech, C., Moutou, C., et al. 2001, A&A, 372, 981  
 Watson, R. A., Rebolo, R., Rubiño-Martín, J. A., et al. 2005, ApJ, 624, L89  
 Werner, M. W., Uchida, K. I., Sellgren, K., et al. 2004, ApJS, 154, 309

## Appendix A: Mid-IR absorption cross-section

In Tab. A.1 we give the parameters defining the mid-IR vibrational bands considered in this work. In all cases we assume their profile to have a Drude shape. The bands at 3.3, 6.2, 7.7, 8.6, 11.3 and 12.7  $\mu\text{m}$  are defined as follows. For the PAH cations, we start from the integrated cross-sections  $\sigma\Delta\nu$  of Pech et al. (2002) which have been derived from laboratory data. The corresponding band profiles, however, do not provide a detailed match of observations. We therefore use band positions and widths as deduced from fits of ISO-SWS spectra of a number of interstellar regions (Verstraete et al. 2001). As indicated by these observations and others (Peeters et al. 2002), we include a broad band at 6.9  $\mu\text{m}$  and split the 7.7  $\mu\text{m}$  into three sub-bands at 7.5, 7.6 and 7.8  $\mu\text{m}$  where we use the observed  $\sigma\Delta\nu$  of each sub-band as weights in defining their integrated cross-sections. In addition, we introduce a band at 8.3  $\mu\text{m}$  to fill the gap between the 7.8 and 8.6  $\mu\text{m}$  bands and multiply the 8.6  $\mu\text{m}$  band by a factor 3 in order to match observations. For neutral PAHs, we use the laboratory integrated cross-section of Joblin et al. (1995) and assume the same band profiles as for the cations. Furthermore, the available spectroscopic data (ISO-SWS, Spitzer -IRS and UKIRT) reveal the presence of other bands at 5.25 and 5.75  $\mu\text{m}$  which have been ascribed to combinations of PAH vibrational modes involving the 11.3  $\mu\text{m}$  band and IR-forbidden modes at 9.8 and 11.7  $\mu\text{m}$  respectively (Roche et al. 1996; Tripathi et al. 2001). For the 5.25  $\mu\text{m}$ , we use the width and intensity ratio to the 11.3  $\mu\text{m}$  band given in Roche et al. (1996). The 5.75  $\mu\text{m}$  band has been derived from the observed spectrum of the Orion Bar (Verstraete et al. 2001). We also added the 17.1  $\mu\text{m}$  band recently seen in Spitzer data (Smith et al. 2004; Werner et al. 2004) and which has been recognized as arising from PAHs (Peeters et al. 2004b; Smith et al. 2007).

## Appendix B: Vibrational modes and density of states of interstellar PAHs

### B.1. Vibrational modes

Symmetric top ( $D_{6h}$  symmetry) type PAHs with  $N_C$  carbon atoms and  $N_H = \sqrt{6N_C}$  hydrogen atoms have  $3(N_C + N_H - 2)$  vibrational modes which can be divided into the following types:  $(N_C - 2)$  out-of-plane (*op*) C-C modes,  $2(N_C - 2)$  in-plane (*ip*) C-C modes,  $N_H$  out-of-plane C-H bending modes,  $N_H$  in-plane C-H bending modes and  $N_H$  C-H stretching (*st*) modes. Following Draine & Li (2001), we approximate the mode spectrum of each type of vibration with a two-dimensional Debye model of maximum energy  $k\Theta$  where  $\Theta$  is the Debye temperature. We derive the mode spectra from the following expressions:

- for the C-C modes:

$$\hbar\omega_i = k\Theta_t \sqrt{\frac{i - \delta_i^t}{N_t}} \quad \text{for } i = 1, N_t \quad (\text{B.1})$$

where  $t = op, ip$  is the type of mode and  $N_t$  is the number of C-C modes of a given type with  $\Theta_{op} = 876$  K and  $\Theta_{ip} = 2318$  K with:

$$\begin{aligned} \delta_i^{op} &= 3/2 \text{ for } i = 2, 3 & \text{and} & \delta_i^{ip} = 1 \text{ for } i = 2, 3 \\ &= 3/4 \text{ otherwise} & & = 1/2 \text{ otherwise} \end{aligned}$$

(B.2)

**Table A.1.** Mid-IR bands of interstellar PAHs adopted in this work for cations and neutrals. The last column indicates the in-plane (*ip*) or out-of-plane (*op*) character of the band (see Sect. 2.2).

$\lambda_i$ ( $\mu\text{m}$ )	$\nu_i$ ( $\text{cm}^{-1}$ )	$\Delta\nu_i$ ( $\text{cm}^{-1}$ )	$\sigma_i/N_H$ ( $10^{-20}\text{cm}^2$ )	$\sigma_i/N_H$ ( $10^{-20}\text{cm}^2$ )	Type
			cations	neutrals	
3.3	3040	39	2.44	10.8	ip
5.2	1905	23	0.58	0.58	op
5.7	1754	60	0.49	0.49	op
8.3	1205	63	1.74	1.74	ip
8.6	1162	47	5.34	0.51	ip
11.3	890	18	17.3	18.3	op
12.0	830	30	3.17	3.17	op
12.7	785	16	5.06	4.06	op
$\lambda_i$ ( $\mu\text{m}$ )	$\nu_i$ ( $\text{cm}^{-1}$ )	$\Delta\nu_i$ ( $\text{cm}^{-1}$ )	$\sigma_i/N_C$ ( $10^{-20}\text{cm}^2$ )	$\sigma_i/N_C$ ( $10^{-20}\text{cm}^2$ )	Type
			cations	neutrals	
6.2	1609	44	2.48	0.52	ip
6.9	1450	300	0.40	0.40	ip
7.5	1328	70	2.70	0.12	ip
7.6	1315	25	1.38	0.06	ip
7.8	1275	70	2.70	0.12	ip
16.4	609	6	1.83	1.83	ip
17.1	585	17	2.48	2.48	ip

- for the C-H modes:

$$\hbar\omega_i = k\Theta_t \sqrt{\frac{3i}{2N_t}} \quad \text{for } i = 1, N_t \quad (\text{B.3})$$

where  $t = op, ip, st$  and  $N_t$  is the number of C-H modes of a given type with  $\Theta_{op} = 1281$  K,  $\Theta_{ip} = 1672$  K and  $\Theta_{st} = 4375$  K.

To this mode spectrum, we add the mode at lowest energy as described in Sect. 2.1. Fig.B.1 shows that our Debye mode spectra is in good agreement with that derived from the Mallocci et al. (2007) database.

### B.2. Density of states and degeneracies

We estimate the PAH density of harmonic vibrational states from direct counts, a mode-to-mode convolution method proposed by Beyer & Swinehart (1973). We start from the rotational density of states, classically given by:  $\rho_{rot}(E) = \sqrt{8E}/B^{3/2}$  with  $E$  and  $B$  in  $\text{cm}^{-1}$  and for a symmetric top (Baer & Hase 1996). We then obtain the rovibrational density of states  $\rho(E)$  with the convolution method. The molecule's zero point energy has been chosen as the zero of the energy scale and the calculation was made for bins with finite width of  $1 \text{ cm}^{-1}$ . To calculate the internal energy distribution of PAHs  $P(E)$ , we grouped this very large number of points into broader energy bins  $[E_i^{min}, E_i^{max}]$  with  $i = 1$  to 500. Each energy bin  $i$  thus contains many states and its degeneracy  $g_i$  is estimated as follows (with  $g_1 = 1$ ):

$$g_i = \int_{E_i^{min}}^{E_i^{max}} \rho(E) dE \quad (i > 1) \quad (\text{B.4})$$

## Appendix C: Behaviour of the rate of $J$ -change for rovibrational emission

We compare here our rates of angular momentum change for rovibrational (IR, see section 4.1) emission to former work and examine the effect of IVR breakdown. We show the absolute value of  $W^+ - W^- = \tau^{-1}\Delta J$  in Fig. C.1. All rates decrease with  $J$  and cross 0 between  $J = 100$  and 150 (the singular point in the curves).

Apart from the damping at high- $J$ , our rate is similar to those of DL98<sup>9</sup> and Ali-Haïmoud et al. (2009). Due to the presence of  $Q$ -bands (rovibrational transitions with  $\Delta J = 0$ ), our damping is lower (by a factor  $\sim 2$ ) and the excitation-to-damping transition ( $\tau^{-1}\Delta J = 0$ ) occurs at higher  $J$ 's.

<sup>9</sup> This rate is corrected as in Ali-Haïmoud et al. (2009).

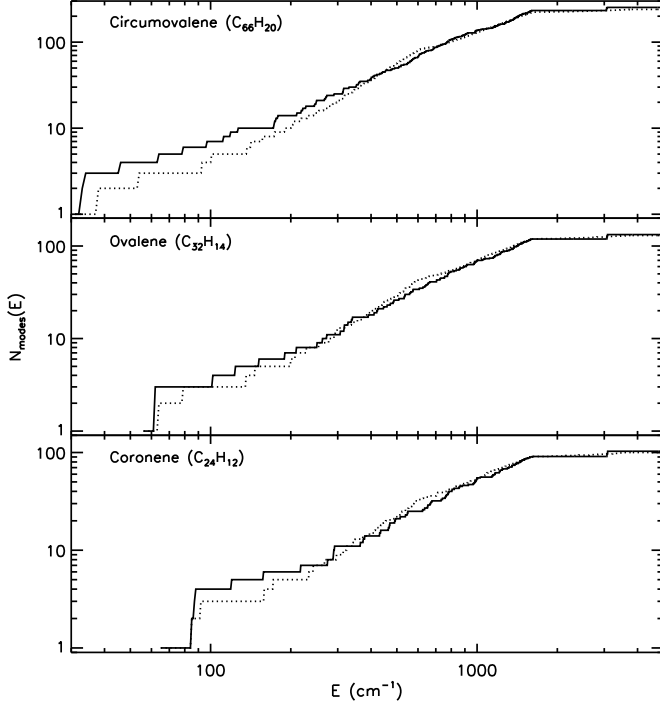


**Fig. B.1.** Cumulative distribution of vibrational modes for coronene ( $C_{24}H_{12}$ ), ovalene ( $C_{32}H_{14}$ ) and circumovalene ( $C_{66}H_{20}$ ) from the Mallocci et al. (2007) database (solid lines) and with our Debye model (dotted lines).

The effect of IVR breakdown is shown in Fig. C.1b. In the extreme IVR cases 1 and 2 (see section 3.1), the IR rate changes on the damping side by a factor 2 and crosses zero at higher- $J$ . For the rotational emissivity of PAHs and including the gas-grain interactions, such differences in the IR rate lead to a peak shift of a few GHz and an intensity change by less than 20%.

## Appendix D: Lines intensities in the rotational bands

In the case of symmetric top molecules, we give below the Hönl-London factors for the angular part of rovibrational transition rates as well as the corresponding transition energies (Herzberg 1968ab). The frequency of the vibrational mode  $i$  is noted  $\nu_{i0}$ .

- for  $\Delta J = 0, \pm 1$  and  $\Delta K = 0$  (parallel transitions or out of plane transitions):

$$\begin{aligned} A_{KJ^+} &= \frac{2((J+1)^2 - K^2)}{(J+1)(2J+1)^2} \quad \text{and} \quad \nu_i^+ = \nu_{i0} - 2B(J+1) \\ A_{KJ^-} &= \frac{2(J^2 - K^2)}{J(2J+1)^2} \quad \text{and} \quad \nu_i^- = \nu_{i0} + 2BJ \\ A_{KJ^0} &= \frac{2K^2}{J(J+1)(2J+1)} \quad \text{and} \quad \nu_i^0 = \nu_{i0} \end{aligned} \quad (\text{D.1})$$

- for  $\Delta J = 0, \pm 1$  and  $\Delta K = \pm 1$  (perpendicular or in plane transitions):

$$\begin{aligned} \left\{ \begin{aligned} A_{KJ^+} &= \frac{(J+2 \pm K)(J+1 \pm K)}{2(J+1)(2J+1)^2} \\ \nu_i^+ &= \nu_{i0} - 2B(J+1) + (B-C)(1 \pm 2K) \end{aligned} \right. \\ \left\{ \begin{aligned} A_{KJ^-} &= \frac{(J-1 \mp K)(J \mp K)}{2J(2J+1)^2} \\ \nu_i^- &= \nu_{i0} + 2BJ + (B-C)(1 \pm 2K) \end{aligned} \right. \end{aligned}$$

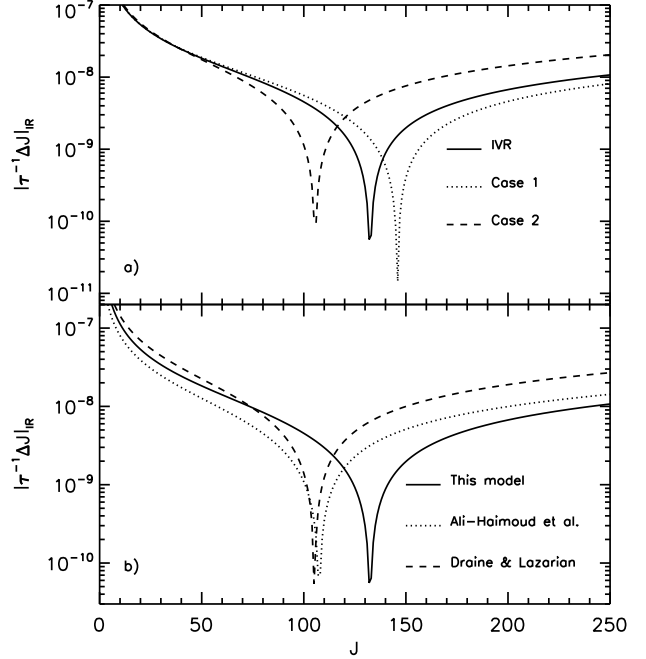


**Fig. C.1.** *a)* Rate of  $J$ -change due to rovibrational emission when IVR is always realized (solid line), in case 1 (dotted line) and in case 2 (dashed line). See sections 3.1 and C for details. *b)* Comparison between our rate of  $J$ -change due to rovibrational emission, solid line, and the rate of DL98 corrected as in Ali-Haïmoud et al. (2009), dashed line, and the rate of Ali-Haïmoud et al. (2009), dotted line.

$$\begin{cases} A_{KJ^0} = \frac{(J+1 \pm K)(J \mp K)}{2J(J+1)(2J+1)} \\ \nu_i^0 = \nu_{i0} + (B-C)(1 \pm 2K) \end{cases}$$

## Appendix E: Rate of angular momentum change for gas-grain interactions

We describe below the gas-grain interactions we take into account in our model of PAH rotation and the rate of change of  $J$ ,  $(\tau^{-1} \Delta J)$ , they induce.

### E.1. Collisions with gas atoms and plasma drag

For the collisions with gas neutrals and ions as well as the plasma drag, we apply the results of DL98 to planar PAHs. In the case where  $J \gg 1$  we use the correspondence principle to write  $\hbar J = I_c \omega$  and obtain the following rates:

$$(\tau^{-1} \Delta J) = -4.1 \times 10^{-10} \sqrt{\frac{T_{\text{gas}}}{100 \text{ K}}} \left( \frac{n_H}{100 \text{ cm}^{-3}} \right) \times J \times F \quad (\text{E.1})$$

for the damping contribution and

$$(\tau^{-1} \Delta J) = 3.1 \times 10^{-5} \left( \frac{T_{\text{gas}}}{100 \text{ K}} \right)^{\frac{3}{2}} \left( \frac{n_H}{100 \text{ cm}^{-3}} \right) \left( \frac{N_C}{50} \right)^2 \times \frac{1}{J} \times G \quad (\text{E.2})$$

for the exciting contribution where  $F$  and  $G$  are normalized rates defined in Appendix B of DL98. We use the formalism of Bakes & Tielens (1994) to estimate the average charge of PAHs of a given size.

### E.2. Rocket effect

Ejection of H or  $H_2$  from the edges of PAHs may yield a significant rotational excitation if it occurs asymmetrically thus generating a systematic torque by the

rocket effect (Rouan et al. 1992). We note below  $E_{ej}$  the kinetic energy of the ejected fragment. In the case of  $H_2$ , this will happen if this molecule forms on preferential sites by chemisorption and if the distribution of these sites on the PAH is asymmetric as a result of dehydrogenation. We calculate the change of  $J$  assuming that  $H_2$  molecules are ejected from the edge of the PAH with a cosine law:

$$(\tau^{-1} \Delta J)_{H_2} = 3.4 \times 10^{-8} \left( \frac{N_C}{50} \right)^{3/2} \left( \frac{n_H}{100 \text{ cm}^{-3}} \right) \times \sqrt{\frac{T_{gas}}{100 \text{ K}}} \sqrt{\frac{E_{ej}}{1.5 \text{ eV}}} (1 - f_H) \text{ s}^{-1} \quad (\text{E.3})$$

The above numerical values are based on the following assumptions: (i) all molecular hydrogen is formed on PAHs with  $[C/H]_{PAH} = 4 \times 10^{-5}$ , a  $H_2$  formation rate  $R_f = 3 \times 10^{-17} (T_{gas}/70\text{K})^{1/2} \text{ cm}^3 \text{ s}^{-1}$  (Jura 1975) and  $E_{ej} = 1.5 \text{ eV}$ ; (ii) the distribution of formation sites has an asymmetry of 1 site and we assume that the site in excess is always at the same location on the molecule; (iii) we neglect the influence of cross-over events that may reduce the angular momentum (Lazarian & Draine 1999). With all these assumptions, the spin rate due to  $H_2$  formation estimated here is an upper limit. This rate is small compared to the other gas-grains processes.

### E.3. Photoelectric effect

UV photons coming from stars are able to pull out electrons from grains. These photoelectrons carry away a significant kinetic energy ( $\sim 1 \text{ eV}$ ) that heats the interstellar gas and impulses grain rotation. If we assume that the photoelectrons leave the grain surface with a cosine law distribution we have:

$$(\tau^{-1} \Delta J)_{pe} = \tau_{pe}^{-1} \times 0.15 \sqrt{\frac{N_C}{50}} \sqrt{\frac{E_{e-}}{1 \text{ eV}}} \text{ s}^{-1} \quad (\text{E.4})$$

where  $\tau_{pe}^{-1}$  is the rate of photoelectrons ejections calculated with the formalism of Bakes & Tielens (1994) ( $\tau_{pe}^{-1} = 1.6 \times 10^{-8} \text{ s}^{-1}$  for  $N_C = 50$ ).